DOI 10.1007/s10946-021-09980-3
Journal of Russian Laser Research, Volume 42, Number 4, July, 2021

NARROW-LINEWIDTH 2128 nm OPTICAL PARAMETRIC OSCILLATOR WITH AN EXTERNAL RESONATOR BASED ON A REFLECTIVE VOLUME BRAGG GRATING

H. Zheng,[1] Z. J. Wang,[1] J. Zhang,[2] Y. H. Wang,[1] G. Y. Jin,[1] and Y. J. Yu[1*]

[1] *Jilin Key Laboratory of Solid-State Laser Technology and Application*
Changchun University of Science and Technology
Changchun 130022, China

[2] *Changchun Guoke Medical Industry Development Technology Co., Ltd.*
Changchun 130000, China

*Corresponding author e-mail: yyjcust@163.com,

Abstract

In this paper, we report an external-cavity 2128 nm narrow-linewidth optical parametric oscillator involving a reflective volume Bragg grating. Based on the Sellmeier equation, we introduce the thermal expansion coefficient together with the thermally-induced output wavelength shift. When the pump power is 12.91 W, with the repetition rate being 70 kHz, a 2128 nm laser with an output power of 3.85 W is obtained, having the optical-to-optical conversion efficiency equal to 30% and the linewidth equal to 108 nm. Moreover, the output power is 2.71 W at 2128 nm and the output linewidth is compressed to 0.19 nm, when a reflective volume Bragg grating is used instead of a total reflection mirror, with the corresponding optical-to-optical conversion efficiency being 21% and the beam quality factor being $M_x^2 = 1.92$ and $M_y^2 = 1.98$. As a result, a 2128 nm narrow-linewidth laser is implemented.

Keywords: optical parametric oscillator, reflective volume Bragg grating, narrow linewidth.

1. Introduction

The narrow-linewidth and high-beam-quality 2.1 μm solid-state laser is widely used in many fields such as medical laser treatment, laser radars, and optoelectronic countermeasures [1–3]. Such laser is also an ideal pumping source for 3–5 μm mid-infrared optical parametric oscillators (OPO). Two approaches are possible in the solid-state laser technology to achieve 2.1 μm radiation. One of them is based on a 1.9 μm laser with Tm rare-earth-ion-doped crystals pumped by a laser diode (LD). The 2.1 μm laser with low quantum defect directly pumped by Ho rare-earth-ion-doped crystals can be implemented [4–7], but both Tm and Ho rare-earth-ion-doped crystals reveal quasi-three-level transitions, and the thresholds are higher than for other crystals, which can cause low conversion efficiency and entail difficulties in operation under high temperatures.

However, there is a simpler and more efficient way involving a degenerate OPO pumped by a 1064 nm solid-state laser, which is based on the nonlinear optical crystal and provides 2.1 μm laser output with high conversion efficiency and high power. In this case, conventional nonlinear optical crystals are employed, such as 1) KTP and KTA crystals based on birefringent phase matching [8–10]; 2) periodically-poled

Manuscript submitted by the authors in English on February 23, 2021.

lithium niobate (PPLN) crystal based on quasi-phase-matching [11–14]. Due to the walk-off effect, the KTP and KTA crystals cannot make use of the maximum effective nonlinear coefficient but, in contrast to the PPLN crystal, which has this technical advantage, especially after doping MgO into the PPLN crystal, the coercive field can be effectively reduced, and the photorefractive damage threshold can be significantly increased.

Biao Wang's research group at the Sun Yat-sen University [15] used 1064 nm intracavity pumping of MgO:PPLN-OPO with an A-O Q-switched Nd:YVO_4 laser. The degenerate 2.1 μm laser output power equal to 3.5 W with a pulse width of 1.4 ns were achieved at a repetition rate of 15 kHz; the optical-to-optical conversion efficiency was 17.5%. Without introducing linewidth controlling devices, the output linewidth was as wide as 30 nm. It was found that. by introducing a volume Bragg grating (VBG) as the output mirror [17], the linewidth of the 2.1 μm laser can be compressed to 2 nm.

However, the employment of a transmission-mode VBG for avoiding direct action of the 1064 nm fundamental light under high power requires introduction of a total reflection mirror for the fundamental-mode light in the OPO cavity. This causes intracavity insertion losses and, at the same time, this indirectly complicates the light path. Also, the high circulating power of the inner cavity and the thermal effect can deteriorate the spectral degeneracy and the beam quality of the 2.1 μm laser. Bearing in mind these problems, MgO:PPLN is taken as the OPO medium under precise temperature control, with a low-loss reflective VBG used to compress the linewidth. In the case of external cavity pumping, 3 W output power at 2.1 μm is obtained, corresponding to the linewidth compression to 0.17 nm with high spectral line degeneracy under 70 kHz repetition rate operation. Horizontal and vertical beam quality factors M^2 factor reach 1.45 and 1.52, respectively.

2. Theoretical Analysis

2.1. VBG Theoretical Analysis

A VBG is used at a particular wavelength that meets the Bragg condition, being reflected into the cavity. The light that does not meet the wavelength condition will leave the cavity. That is the key idea for the linewidth compression, as shown in Fig. 1.

According to the coupled-wave theory developed by Kogelink in 1969, the diffraction efficiency and diffraction linewidth of a reflective volume Bragg grating can be accessed. When the VBG thickness is greater than 5 mm, as shown in Fig. 2, the diffraction efficiency of the VBG is close to 100%, which means higher spectral selectivity. When taking an OptiGrate VBG with a thickness of 20 mm, the simulated linewidth is 0.11 nm.

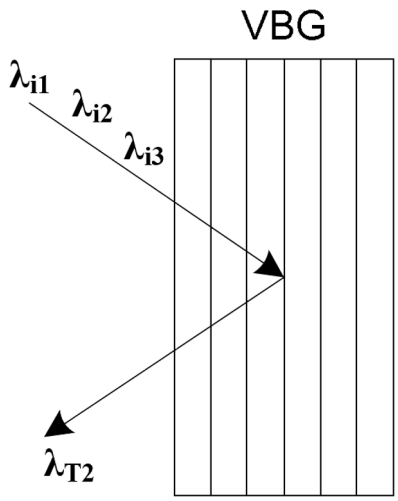

Fig. 1. Schematic diagram of the volume Bragg grating.

2.2. Theoretical Analysis of the Effect of Crystal Thermal Expansion for PPLN

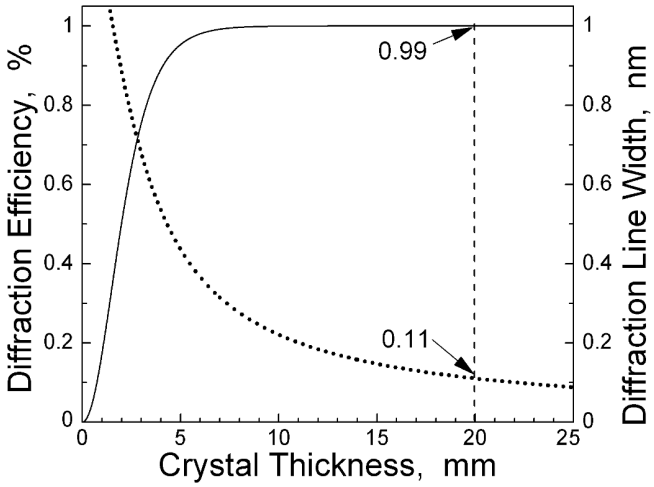

Fig. 2. Dependences of the diffraction efficiency (the solid curve) and diffraction linewidth (the dotted curve) on the crystal thickness.

According to the theoretical analysis and Sellmeier equation, the quasi-phase matching condition is given as

$$\frac{n_p}{\lambda_p} - \frac{n_s}{\lambda_s} - \frac{n_i}{\lambda_i} - \frac{1}{\Lambda_{\mathrm{PPLN}}} = 0. \tag{1}$$

In this formula, Λ_{PPLN} is the poling period of the crystal, λ_p, λ_i, and λ_s are the wavelengths of pumping light, idler beam, and signal light, n_p, n_i, and n_s are the respective refractive indices for the pumping light, idler beam, and signal light in the crystal medium. In Fig. 3, we show the relation between the output wavelength and temperature for different poling periods for the PPLN crystal.

Due to a limited range of the temperature controlling device, low temperatures are not conducive to the degeneracy point. The poling period used in this experiment is 23.25 μm, and based on this fact, the thermal effect is added to the degeneracy point,

$$T(r,z) = -\frac{r^2}{w_p^2}\frac{\alpha P_{\mathrm{ph}}\exp(-\alpha z)}{2\pi K_c}, \tag{2}$$

Crystal thermal conductivity rate K_c is 0.046 W/mm·K, if we set the distance from the focal point of the optical axis to the optical axis radius r within the end face of the crystal as 3 mm, the pump power P_{ph} is 40 W, the spot radius w_p is 0.5 mm, the crystal absorption coefficient α is 0.005, and the crystal length z is 50 mm.

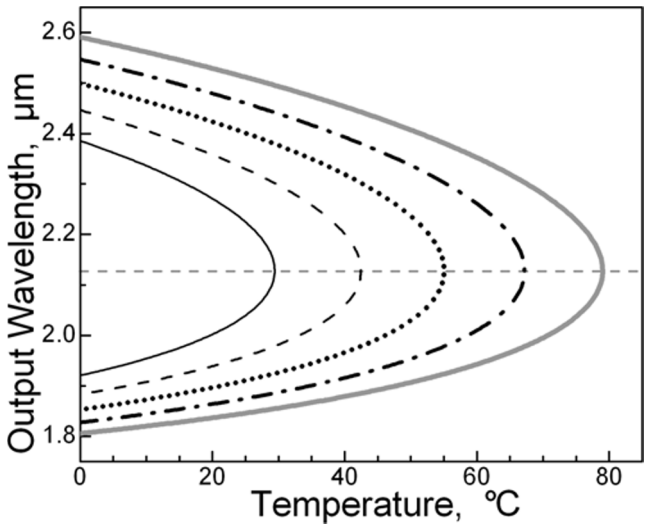

Fig. 3. Temperature tuning for poling periods equal to 23.35 μm (the solid curve), 23.30 μm (the dashed curve), 23.25 μm (the dotted curve), 23.20 μm (the dash-dotted curve), and 23.15 μm (the gray curve).

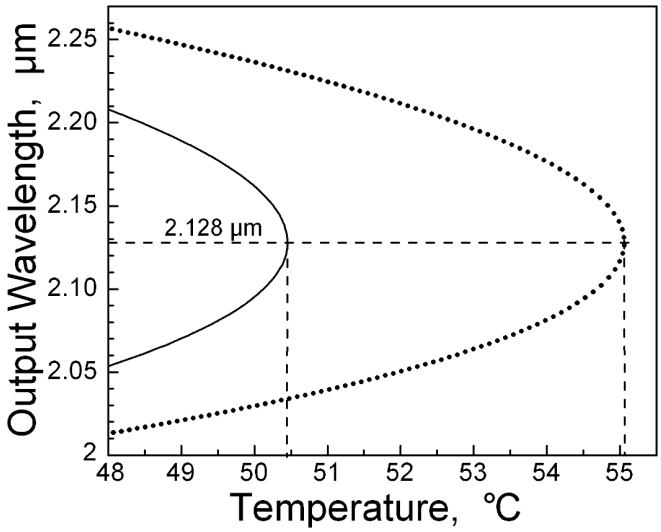

Fig. 4. The output wavelength versus temperature with (the solid curve) and without (the dotted curve) the thermal expansion coefficient added.

The crystal poling period at temperature T can be expressed as

$$\Lambda(t) = \Lambda(t_0)g[1 + c(t - t_0)], \tag{3}$$

where $\Lambda(t_0)$ is the poling period of the crystal at room temperature T_0, $c = 2.0 \cdot 10^{-6}\mathrm{K}^{-1}$ is the thermal expansion coefficient of the crystal, $T = T_1 + T_2$, with T_1 being the elevated temperature due to the absorption of the pump light by the MgO:PPLN crystal.

After substituting (7) into (6), we arrive at the final expression and perform simulations; the results are shown in Fig. 4. After adding the thermal expansion coefficient, the corresponding temperature of the degeneracy point is 50.5°, and the temperature corresponding to the degeneracy point with the thermal expansion coefficient disregarded is 55.2°.

Due to the crystal thermal expansion after irradiation by the pump light and heating by the temperature control furnace, the poling period of the crystal is increased, which causes a reduction in the temperature corresponding to the degeneracy point by 4.6°. One can see that the disregard of the thermal effect in the crystal results in an inaccurate prediction of the degeneracy point temperature in the subsequent experimental process.

3. Experimental Setup

In Fig. 5, we show the external-cavity MgO:PPLN-OPO experimental device based on a reflective VBG. A high-repetition-rate A-O Q-switched Nd:YVO_4 laser pumped at 808 nm by an LD fiber coupling module is used as the pumping source to obtain the 1064 nm fundamental-mode light. The resonator is a folded cavity, M1 is a total reflection mirror coated with a film having total reflection at 1064 nm, and M2 is a 45° spectroscope coated with an 808 nm antireflection film and a 1064 nm total reflection film. The 808 nm pump light passes through a 1:2 coupling lens group (transmission coupling efficiency is 97%) and pumps the bonding-type Nd:YVO_4 crystal after being focused. An aperture is introduced between lenses M1 and M2 in the folded cavity structure to suppress the higher-order mode oscillations. The mode volume is also increased and the pump spot matching is improved. M3 is an output mirror

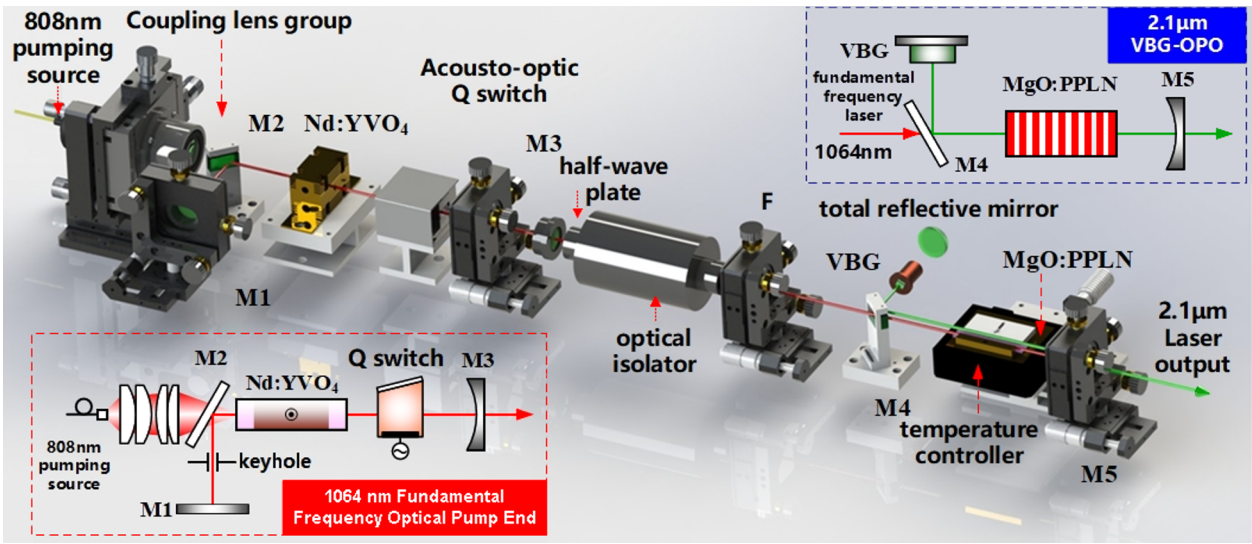

Fig. 5. Schematic diagram of the experimental setup.

with 60% transmittance at 1064 nm. The RF power of the acousto-optic Q-switch is 20 W, with the frequency being 40.68 MHz, whereas diffraction loss is more than 90%. To reduce the transit time of ultrasonic waves in the acousto-optic medium, the A-O Q-switch is placed on the side close to the output mirror M3. At a repetition rate of 70 kHz and maximum pump power of 54 W, the average output power at 1064 nm is 15.7 W, with the pulse duration being 9.43 ns, and the beam quality factor $M^2 < 1.25$.

Linearly polarized fundamental-frequency output laser radiation passes through a half-wave plate for adjusting the polarization direction and enters a free-space isolator (model IO-8-1064-HP produced by Thorlabs). A lens F with a focal length of 150 mm is placed between the isolator and the external-cavity OPO to focus and couple the fundamental-frequency laser (1064 nm) into the MgO:PPLN polar crystal. The crystal size is $3\times3\times50$ mm^3 and the poling period is 32.25 μm. The crystal is placed in an OV50 temperature controller produced by Taiwan HCP Company; the temperature control accuracy reaches 0.1°. Two end faces of the crystal are coated with a 1064 and 2128 nm two-color antireflection film. The reflective VBG produced by OptiGrate is used instead of the external-cavity OPO total reflection mirror M6 coated with a 2128 nm total reflection film. The VBG modulation wavelength is adjusted at 2128 nm, with an aperture of 6×6 mm^2. To obtain higher diffraction efficiency, the thickness of the VBG is chosen to be 20 mm to prevent the direct effect of the high-power fundamental-frequency laser on the VBG. The external-cavity OPO is designed as an "L" cavity with a length of 160 mm. The plane mirror M4 is placed at 45° coated with a 1064 nm antireflection film and a 2050–2150 nm "S"-polarized total reflection film. The output mirror M5 is a plane-concave mirror with a curvature radius of 200 mm, coated with a 1064 nm high-reflection film and a 2050–2200 nm partial transmission film; reflectivity is $R \approx 50\%$.

4. Experimental Results and Analysis

As shown in Fig. 5, the experiment involves M6 as the total reflection mirror and M5 as the output mirror with a curvature radius of 200 mm. The transmittances are 50% and 60%, respectively. The experimental results are shown in Fig. 6. When maximum pump power is 12.91 W and $T = 50\%$, a

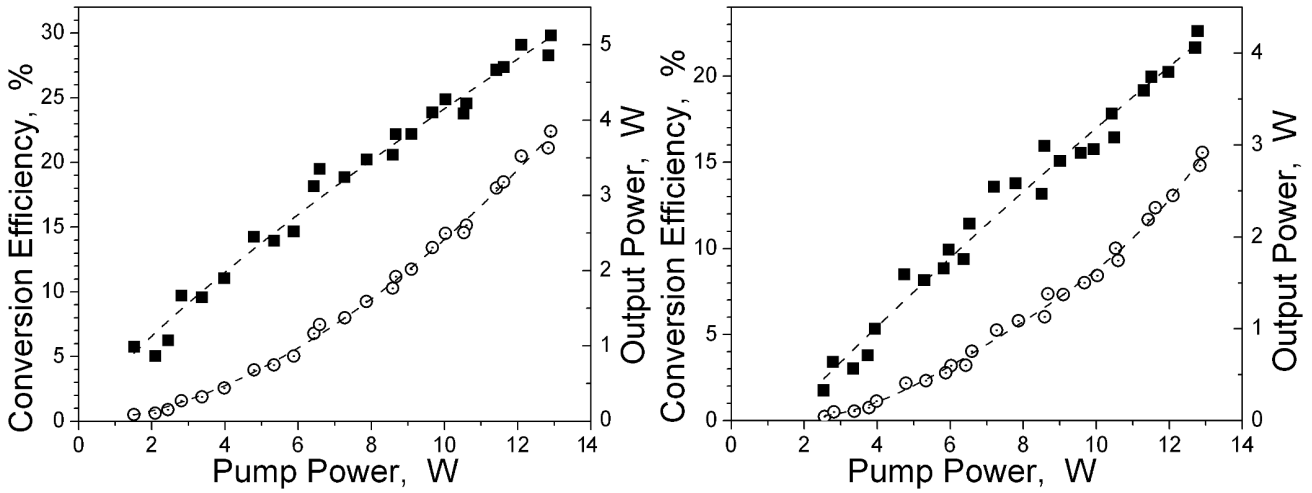

Fig. 6. Output power (⊙) and conversion efficiency (■) at 2.1 μm versus the laser diode power in free operation. Here, $T = 50\%$ (a) and $T = 60\%$ (b).

maximum output power is up to 3.85 W and an optical-to-optical conversion efficiency is 29.8%. When $T = 60\%$ is taken, the maximum output power of 2.92 W and the optical-to-optical conversion efficiency of 22.2% are achieved.

For $T = 50\%$, the output power is higher than that for $T = 60\%$, so the output mirror with $T = 50\%$ is used in the subsequent experiments.

Then, a spectrum analyzer AQ6375 from Japan Yokogawa with ±0.05 nm wavelength precision and 1200 – 2400 nm spectral range is used to measure the output wavelength of parametric light at different temperatures. The results are shown in Fig. 7. where one can see that, when the temperature controller is set to 50.5°, the linewidth of degenerate light is as wide as 108 nm. After adding a VBG, the linewidth of degenerate light is compressed to 0.18 nm; see Fig. 8. The linewidth is compressed but, due to the VBG placement angle and material processing errors, there is an error of 0.11 nm with respect to the simulated diffraction linewidth.

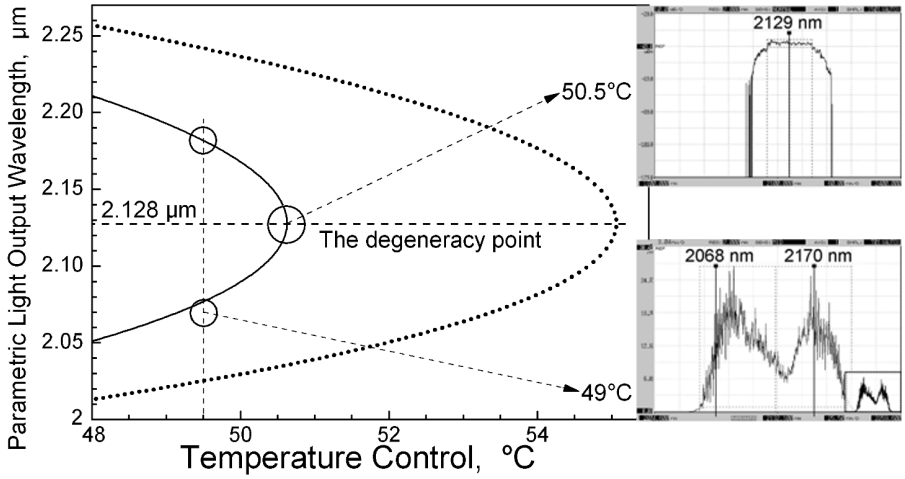

Fig. 7. the output wavelength versus temperature for simulation with (the solid curve) and without (the dotted curve) taking into account thermal effects.

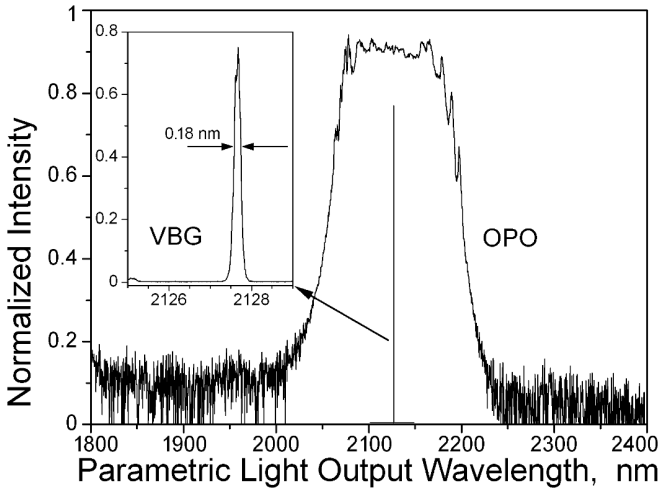

Fig. 8. 2128 nm degenerate point OPO output spectrum.

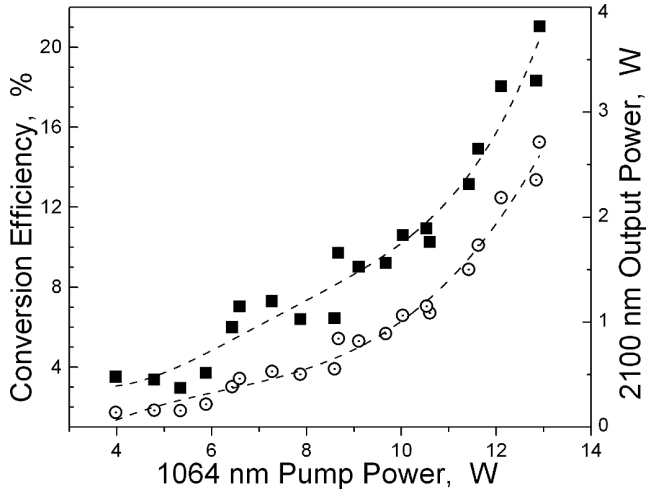

Fig. 9. 2.1 μm output power after adding VBG (⊙) and the conversion efficiency (■) versus the laser diode power.

Under the same experimental conditions, when a VBG is used as the total reflection mirror to compress the linewidth, the conversion efficiency of the 2128 nm laser is reduced since the VBG can transmit light without meeting the Bragg diffraction conditions. The highest output power of the 2128 nm laser after adding the VBG is 2.71 W, corresponding to the optical-to-optical conversion efficiency of 21%. As shown

in Fig. 9, the output power of the 2128 nm laser reveals no visible saturation, which means that the power can be further improved.

In Fig. 10, we show the 2128 nm laser pulse diagram at a repetition rate of 70 kHz; the average pulse width of the laser is 14.75 ns.

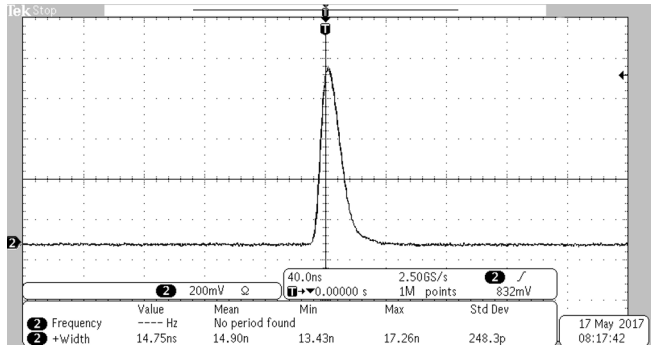

Fig. 10. Pulse width of the 2128 nm laser at a 70 kHz repetition rate.

A pyroelectric array camera Pyrocam III, Israel OPHIR was used to measure the laser spot of the 2128 nm laser after placing a 200 mm focusing lens in the parametric-light transmission direction. After measuring the laser spot size at different positions behind the focusing lens by 90/10 knife cutting and fitting the beam waist radius and far-field divergence angle according to the Gaussian-beam propagation equation, the quality factor M^2 of the measured beam is calculated as $M_x^2 = 1.92$ and $M_y^2 = 1.98$; see Fig. 11.

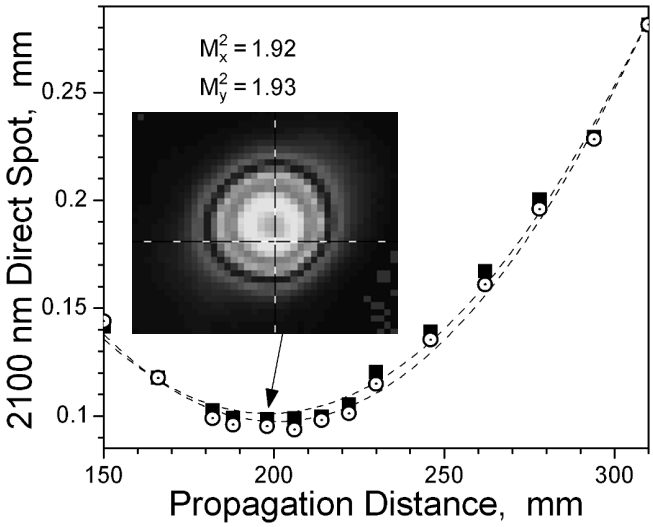

Fig. 11. Spot pattern and beam quality fitting for the 2128 nm laser for the x (■) and y (⊙) directions.

5. Conclusions

Based on the MgO:PPLN crystal and using a pulse-pumped external cavity optical parametric oscillator with a reflective volume Bragg grating, we introduced the thermal expansion coefficient based on the Sellmeier equation. In addition, our study of the MgO:PPLN crystal after pump light irradiation and heating by the temperature controller showed that thermal expansion results in increase in the poling period of the crystal and decrease in the degeneracy point by 4.6°. Setting the temperature to 50.5° in the temperature controller, with a pump power of 12.91 W and a repetition rate of 70 kHz, we obtained a narrow-linewidth 2128 nm laser with the output power equal to 2.71 W. Under the conditions described, the linewidth is 0.18 nm and the optical-to-optical efficiency is 21%. Also, for the beam quality factor, we obtained values $M_x^2 = 1.92$ and $M_y^2 = 1.98$. Thus, we provided a technical method for the implementation of a 2128 nm narrow-linewidth laser.

Acknowledgments

The work is supported by the National Natural Science Foundation of China under Grant Nos. 61505001 and 11974060, China Postdoctoral Science Foundation under Grant No. 2016M591466, the Key Scientific and Technological Research Project of the Jilin Provincial Department of Science and Technology (approval number 20170204046GX), and a Project funded by the Young and Middle-Aged Scientific and Technological Innovation Leaders and Team of the Jilin Provincial Department of Science and Technology (approval number 20190101004JH).

References

1. J. Guo, G.-Y. He, Z.-X. Jiao, et al., *J. Infrared Millim. Waves*, **33**, 625 (2014) [in Chinese]; DOI: 10.3724/sp.j.1010.2014.00625
2. Z. Jiao, G. He, J. Guo, and B. Wang, *Opt. Lett.*, **37**, 64 (2012).
3. O. A. Buryy, D. Y. Sugak, S. B. Ubizskii, et al., *Appl. Phys. B*, **88**, 433 (2007).
4. X.-J. Cheng, J.-Q. Xu, W.-X. Zhang, et al., *Chinese Phys. Lett.*, **26**, 130 (2009).
5. X. L. Zhang, Y. Z. Wang, L. Li, and Y. L. Ju, *Acta Phys. Sin.–Ch. Ed.*, **04**, 2196 (2007).
6. M. Qing-Lei, Z. Nan, X. Shi-Yong, et al., *Chinese Phys. Lett.*, **26**, 124211 (2009).
7. Z. Yu-Wan, Z. Yong-Dong, Z. Xin, et al., *Chinese Phys. Lett.*, **27**, 144 (2010).
8. P. B. Phua, B. S. Tan, R. F. Wu, et al., *Opt. Lett.*, **31**, 489 (2006).
9. Q. J. Cui, Y. T. Xu, N. Zong, et al., *Acta Phys. Sin.–Ch. Ed.*, **58**, 1715 (2009).
10. B. Jacobsson, V. Pasiskevicius, F. Laurell, et al., *Opt. Lett.*, **34**, 449 (2009).
11. D. Xin, Z. Shao-Min, M. Hong-Mei, et al., *Chinese Phys. B*, **017**, 211 (2008).
12. M. Henriksson, L. Sjöqvist, V. Pasiskevicius, and F. Laurell, *Appl. Phys. B*, **86**, 497 (2007).
13. P. Blau, S. Pearl, S. Fastig, and R. Lavi, *IEEE J. Quantum Electron.*, **44**, 867 (2008).
14. D. Li, Y. Yu, Y. Li, et al., *Opt. Laser Technol.*, **131**, 106412 (2020).
15. J. Saikawa, M. Fujii, H. Ishizuki, and T. Taira, *Opt. Lett.*, **32**, 2996 (2007).
16. G. Jing, H. Guang-Yuan, J. Zhong-Xing, and W. Biao, *Acta Phys. Sin.–Ch. Ed.*, **64**, 182 (2015).
17. J. Guo, G. He, B. Zhang, et al. *IEEE Photonics Technol. Lett.*, **27**, 573 (2015).